Nonadiabatic State-to-State Reactive Collisions among Open Shell Reactants with Conical Intersections: The OH($^2\Pi$) + F(^{2}P) Example†

Alexandre Zanchet,‡ Tomás González-Lezana,‡ Alfredo Aguado,§ Susana Gómez-Carrasco,‡,|| and Octavio Roncero*,‡

Unidad Asociada UAM-CSIC, Instituto de Física Fundamental, CSIC, Serrano 123, 28006 Madrid, Spain, Unidad Asociada UAM-CSIC, Departamento de Química Física, Facultad de Ciencias C-XIV, Universidad Autónoma de Madrid, 28049 Madrid, Spain, Theoretical Chemistry Department, Institute of Physical Chemistry, University of Heidelberg, Im Neuenheimer Feld 229, D-69120 Heidelberg, Germany

Received: March 3, 2010; Revised Manuscript Received: April 28, 2010

Accurate wave packet calculations on the OH($^2\Pi$) + F(^{2}P) → O(^{3}P) + HF($^1\Sigma^+$) reactive collisions are performed using a recently proposed coupled diabatic states. Adiabatic and nonadiabatic dynamics are compared in detail, analyzing the final state distribution of products. It is found that with the new surfaces a significant increase of the rate constant is obtained, with noticeable nonadiabatic effects. The inclusion of the spin−orbit splittings for the calculation of the electronic partition function produces an important increase of the reaction rate constants, yielding a rather good agreement with the experimental results. It is also concluded that spin−orbit couplings are also necessary in the entrance channel to describe this reaction.

I. Introduction

The presence of open shell systems in an ample variety of processes such as combustion, plasmas, atmosphere, and interstellar media is quite common.[1] In the atmosphere, for example, the photodissociation of ozone, a key ultraviolet filter, yields products in different electronic states, $O_2(^1\Delta_g,^3\Sigma_g^-,^3\Sigma_u^+,^3\Delta_u)$ + O(^{3}P,^{1}D). Thus, several electronic states participate in the dynamics, which present conical intersections (CI) and electronic transitions, making it necessary to treat nonadiabatic dynamics in a diabatic representation, as studied in detail by Schinke and co-workers.[2,3] The open shell oxygen atoms collide with other species of great importance in atmospheres,[4] such as NO($^2\Pi$),[5] involving several asymptotically degenerate electronic states. One of the most studied reactions is the O + H_2 case. Due to its interest in combustion, the nonadiabatic dynamics has been the subject of a large number of theoretical investigations.[6−13] The corresponding electronic states may cross along the minimum energy path (MEP) involved in the collision, leading to CI's, at which nonadiabatic couplings should play an important role in the dynamics. Despite the frequent occurrence of such CI's, there are only a few processes for which accurate coupled diabatic potential energy surfaces (PES's) are available to account for the full collision.

A good example of such exceptions are the reactions between an oxygen atom in its ground ^{3}P or excited ^{1}D electronic states with hydrogen halides, O + HX. The most important and more studied of these reactions, crucial in the catalytic ozone destruction cycle, is that involving chlorine atoms,[14−24] typically in single adiabatic PES's. On the other hand, the analogous OHF system constitutes a benchmark case, because its relative simplicity allows very accurate ab initio calculations. Recently, two coupled diabatic PES's have been proposed[25] for the OH($^2\Pi$) + F(^{2}P) ↔ O(^{3}P) + HF($^1\Sigma^+$) reaction, which shows CI's around the reaction barrier, as displayed in Figure 1.

Experimental information about OHF was obtained in the photoelectron detachment spectroscopic studies performed by Neumark and co-workers.[26−28] In these experiments the OHF^- anion, of linear equilibrium configuration, is excited by detaching an electron, and several electronic states of the neutral OHF system are reached in the region of the transition state. More recently, Continetti and co-workers[29,30] have detected in coincidence the electron and neutral fragments. Since the formation of products requires the wave packet (WP) to pass through CI's, such experimental data provide direct detailed information about nonadiabatic transitions.

Initially, several theoretical simulations of the photodetachment spectrum were performed restricted to collinear OHF geometries and the ground electronic state.[26,31] Later, three-dimensional (3D) PES's for the ground triplet $1^3A''$ state[32] and the two first excited triplet states, $2^3A''$ and $1^3A'$, were obtained.[33] The simulated photodetachment spectra,[34] obtained using these three 3D PES's of the lower triplet states, and four two-dimensional PES's for singlet states, reproduced qualitatively rather well all the structures of the experimental photoelectron detachment spectrum.[26] More recently, coupled 3D diabatic PES to describe the three triplet states of OHF[25] and the 3D PES's of the five singlet states of OHF (correlating to the O(^{1}D) + HF)[35] were obtained and applied to simulate the photodetachment experiments.

Regarding collisions processes, arrested infrared chemiluminescence[36] and kinetic[37] experimental studies on the OH($^2\Pi$) + F(^{2}P) reaction have been carried out, but there are no results on the reverse reaction due to its endoergicity, of about 1.5 eV (see Figure 1). Open shell species are obtained in low densities and cross beam experiments become very difficult to perform. The reactive collisions were first studied using quasi-classical trajectory (QCT) and WP methods on a single adiabatic PES.[32,38] Later the calculations were extended to consider the three adiabatic states (2 of $^3A''$ and 1 of $^3A'$ symmetry) and the thermal rate constants were obtained combining WP and QCT

† Part of the "Reinhard Schinke Festschrift".
* Corresponding author. E-mail: ORoncero@iff.csic.es.
‡ CSIC.
§ Universidad Autónoma de Madrid.
|| University of Heidelberg.

10.1021/jp101914a
Published on Web 05/13/2010

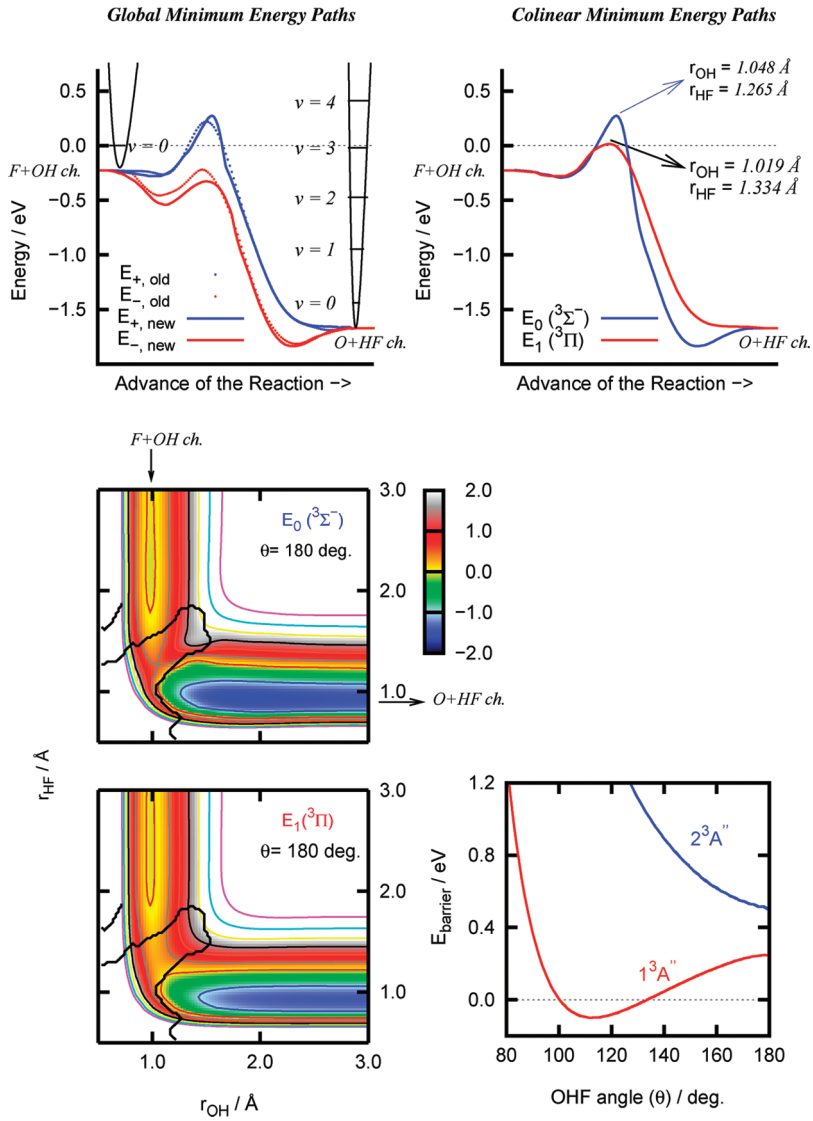

Figure 1. Top: minimum energy path in eV: (left) for the adiabatic $1^3A''$ and $2^3A''$ states resulting from the regularized diabatic states of ref 25 and the old adiabatic fits of refs 32 and 33; (right) for the diabatic $^3\Sigma^-$ and $^3\Pi$ states at a collinear geometry. Bottom: (left) contour plots of the two diabatic $^3\Sigma^-$ and $^3\Pi$ states at OHF collinear geometry, indicating with a black line the conical intersection seams; (right) angular dependence of the adiabatic $1^3A''$ and $2^3A''$ states, at $r_{OH} = 1.019$ Å and $r_{HF} = 1.334$ Å, approximately the saddle point of the ground adiabatic state.

calculations. The rates thus obtained, when multiplied by the electronic partition function (3/24, the 3 arising by the degeneracy of each triplet state, and considering no spin−orbit splitting), are too low as compared with the experimental one.[37] This was attributed to the neglect of the nonadiabatic couplings arising among the three triplet states, which are very important at the CI's appearing along the MEP (see Figure 1). Very recently, the $H(^2S) + FO(^2\Pi) \rightarrow (OH(^2\Pi) + F(^2P))/(HF + O(^3P))$ exoergic reaction has been studied using WP[39,40] and QCT[40−42] methods, making emphasis on the electronic branching ratio and the stereodynamics.

The aim of this work is to investigate the nonadiabatic $OH(^2\Pi) + F(^2P) \rightarrow O(^3P) + HF(^1\Sigma^+)$ reactive collisions and to determine the role played by the CI's, checking if this could be the reason for the disagreement found between theory and experiment.[33] For this purpose, the coupled diabatic PES's developed previously[25] will be used to perform WP calculations to evaluate state-to-state cross sections, comparing with the same results obtained with the corresponding adiabatic PES's and with the available experimental data. Also the rate constants are calculated including the spin−orbit splitting of the reactants.

The paper is organized as follows. In section II, the computational details and the PES's are described. In section III, the results are described and discussed. Finally, section IV is devoted to extract some conclusions.

II. Numerical Simulation

$OH(v=0,j=0) + F \rightarrow O(^3P) + HF(v',j')$ reactive collisions are simulated using a WP method described in detail in refs.[43−47] For this system it has been demonstrated that it is more efficient to use product Jacobi coordinates[46] because of the HL + H′ → H + LH′ mass combination. Thus prod-WP calculations have been done with the MAD-WAVE3 code described in ref 47, and the parameters used in the propagations are listed in Table 1.

Calculations have been conducted for some selected total angular momenta, $J = 0$, 10, 20, 30, ..., 120, for all the electronic states described below in the diabatic and adiabatic representations. Ten helicity components, $\Omega = 0$, ..., 9 were included and the convergence obtained for the test cases of $J = 30$, 60, and 90 is better than 1%. The largest errors correspond to long-

TABLE 1: Parameters Used in the Wave Packet Calculations in Product Jacobi Coordinates

r_{min}/Å	0.4	A_R/Å^{-2}	0.035
r_{max}/Å	13	N_γ	280 in [0, π]
N_r	256	R_0/Å	10
r_l/Å	11	E_0/eV	0.25
A_r/Å^{-2}	0.01	ΔE/eV	0.125
R_{min}/Å	0.75	R'_∞	11
R_{max}/Å	13	V_{cut}/eV	2
N_R	420	E^l_{cut}/eV	5
R_l/Å	11		

lived resonances appearing at low energies for moderately low J. For safe computing time, the reaction probabilities at intermediate J's were obtained by an interpolation procedure based on the J-shifting approach:[48] for a given J value (with $J_1 \leq J \leq J_2$) the reaction probability is obtained as

$$P_J(E) = \frac{J - J_1}{J_2 - J_1} P_{J_1}(E - B[J(J+1) - J_1(J_1+1)]) + \frac{J_2 - J}{J_2 - J_1} P_{J_2}(E + B[J_2(J_2+1) - J(J+1)]) \quad (1)$$

where the rotational constant B is previously fitted. Thus, the state-to-state integral cross sections are obtained by summing over J, requiring a maximum value of $J = 120$ for 0.57 eV of collision energy.

The coupled regularized diabatic PES's used for this reaction were proposed previously.[25,49] The three electronic states correlating with the O(^{3}P) + HF products also correlate with the OH($^2\Pi$) + F(^{2}P) reactants. In an adiabatic representation these states separate in two ^{3}A″ and one ^{3}A′ states, corresponding to the C_s symmetry group of the system. In the diabatic representation defined in ref 25, the states are chosen to match the adiabatic eigenstates at collinear geometry and can be labeled using the $C_{\infty v}$ group symmetry classes as $^3\Pi$ and $^3\Sigma^-$ in the present case. This different notation for adiabatic and diabatic states will be used hereafter to distinguish between them. Since they are all degenerate at the two asymptotes, they are nearly parallel along the MEP, and they cross, as shown in Figure 1. In an adiabatic representation such crossings are avoided at bent geometries, but at collinear configurations these states separate in different symmetries and they can cross, giving rise to CI's, at which the nonadiabatic couplings diverge.[25] These CI's are close to the transition state region and are expected to play a fundamental role in the reaction dynamics.[25,34] In fact, the ground adiabatic 1^{3}A″ state presents two wells, in reactant and product channels, and the lowest reaction barrier, which is slightly bent because of the $\Sigma-\Pi$ coupling.[34]

Moreover, the CI's appearing in the adiabatic representation between the two ^{3}A″ states, give rise to cusps, which are difficult to fit. Thus, the adiabatic states obtained after diagonalizing the 2 × 2 diabatic matrix reproduce these cusps much better than the previously proposed PES for the ^{3}A″ states,[25,32,38] as can be seen in Figure 1. However, the excited 1^{3}A′ state does not present any crossing for this symmetry, and the best available PES is that described in ref 33. This state is only coupled to the other two by electronic Coriolis, Renner−Teller and spin−orbit couplings, neglected in this work. Since this state yields to very small cross sections[33] it will not be taken into consideration hereafter.

In this work we focus on the nonadiabatic effects. For this reason we present calculations in the diabatic (formed by the coupled $^3\Sigma^-$ and $^3\Pi$ states) and in the adiabatic representation (for the two independent 1^{3}A″ and 2^{3}A″ states), starting in each of the two electronic states of each representation. Note that the adiabatic states used here arise from the diagonalization of the 2 × 2 diabatic matrix and reproduce the cusps due to the CI, in contrast to the previous ones.[32,33,38] Thus, the barriers are considerably different, as will be described below.

HF + O(^{3}P) products correspond to an open shell atom and a closed-shell diatomic molecule. In the diabatic representation formed by the $^3\Sigma^-$ and $^3\Pi$ states, the electronic orbital angular momentum ($\Lambda = 0$ and 1, respectively) is well described and the Hamiltonian of Rebentrost and Lester[50] is used in the dynamical calculations. In the adiabatic representation, however, the electronic angular momentum corresponds to a mixture, and it is neglected using the typical Hamiltonian for closed shell fragments.

It should be noted that OH($^2\Pi$) + F(^{2}P) reactants correspond to open shell atom and diatom for which the Hamiltonian of Rebentrost and Lester[50] is not well adapted. A better description should consider a more complete electronic diabatic basis set, formed by all the states correlating with reactants and products. This would imply other states, correlating to the O(^{1}D) + HF($^1\Sigma^+$) and O(^{3}P) + HF($^3\Pi$), to be included, which is not the scope of this work.

III. Dynamical Results and Discussion

1. Zero Total Angular Momentum, $J = 0$. The total reaction probabilities obtained for $J = 0$ and each of the two initial adiabatic and diabatic states are shown in the bottom panel of Figure 2, together with the corresponding sums. The adiabatic results are qualitatively similar to those previously reported for the older PES's.[32,33] The reaction probability for the ground 1^{3}A″ state in refs 32 and 33 presents resonances at the threshold, which were attributed to H−L−H resonances of the light H atom among the two heavier atoms in the well of the entrance channel,[32] followed by a sudden increase, at ≈0.07 eV, associated with a direct reaction mechanism. In the present case, there is nearly no separation between the two regions, and the resonant structure is superimposed on the envelope of the direct mechanism, while in the older PES there was a net separation between them. This difference is attributed to the lower energy barrier of the new PES's due to the better description of the cusps of the CI's.

The reaction probability associated with the excited adiabatic 2^{3}A″ state is shifted toward considerably higher energy and is considerably lower (note that in the figure is multiplied by 5), as it was also the case obtained for the older PES.[33] For this state the reaction is direct, and there are no oscillating structures associated with resonances.

In the diabatic representation the situation is rather different. First, the reaction probabilities present the same energy threshold for the two initial electronic states. This is consistent with the fact that in the adiabatic representation the ground state accounts for nearly all the reactivity.

In the diabatic representation, the reaction probabilities obtained for the system initially in the $^3\Sigma^-$ or $^3\Pi$ diabatic states are very similar. The sum of the two probabilities is considerably higher, by a factor of about 4/3, than that obtained in the adiabatic representation, for energies above 0.2 eV. Also, in the lower energy range where the resonant structure dominates, the total reaction probability obtained in the diabatic representation is considerably higher than in the adiabatic representation. Only at energies on the order of 0.07 eV do the two representations yield similar results. This demonstrates the high probability of electronic transitions in the diabatic representation.

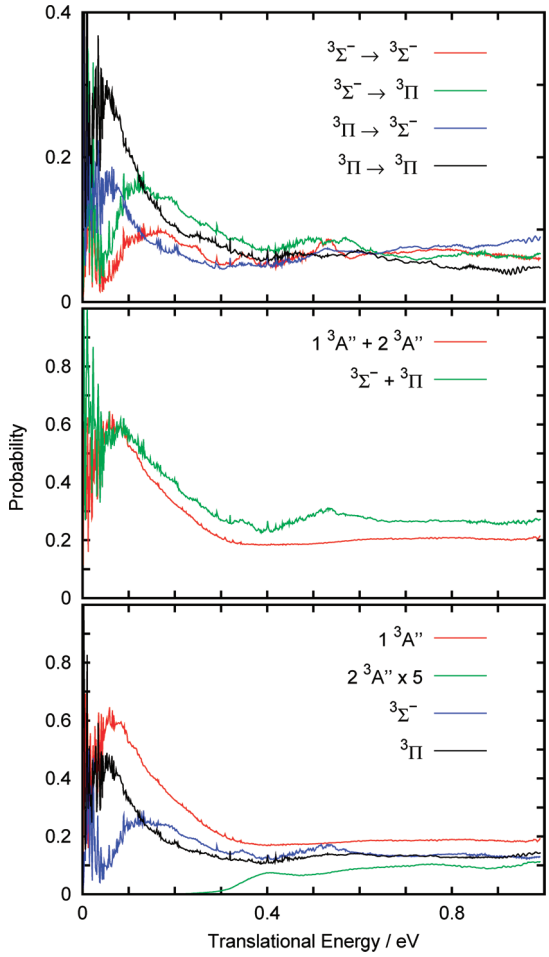

Figure 2. Reaction probabilities obtained for F + OH(v=0,j=0) reactive collision at zero total angular momentum, J = 0, for the adiabatic and the diabatic representations. Bottom panel: total reaction probabilities obtained for the adiabatic $1^3A''$ and $2^3A''$ (this case multiplied by 5) and diabatic $^3\Sigma^-$ and $^3\Pi$ states. Middle panel: total reaction probabilities in the diabatic and adiabatic representations as a sum of those shown in the bottom panel. Top panel: diagonal and nondiagonal reaction probabilities obtained in the diabatic representation, for the two initial and final electronic states.

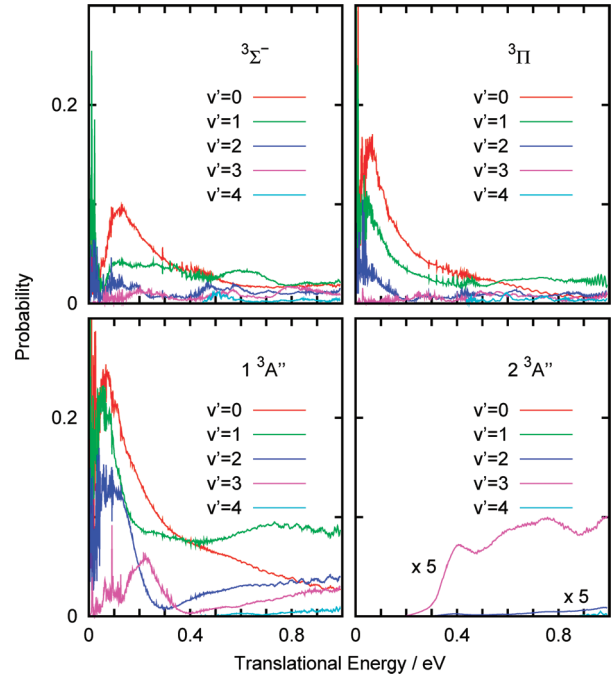

Figure 3. Final vibrational reaction probabilities for F + OH(v=0,j=0) → O(^{3}P) + HF(v') reactive collision at zero total angular momentum, J = 0, calculated for each initial electronic state in the diabatic (top panels) and adiabatic (bottom panels) representations. Note that probabilities in the bottom right panel are multiplied by 5.

This argument is confirmed by the final electronic distribution of the HF products, shown in the top panel of Figure 2. In the low energy range below 0.5 eV, the direct reaction in the $^3\Sigma^-$ → $^3\Sigma^-$ state is not possible because its high reaction barrier, and two electronic transitions must occur to end in the $^3\Sigma^-$ state: first, $^3\Sigma^-$ → $^3\Pi$ to overpass the reaction barrier, and a second $^3\Pi$ → $^3\Sigma^-$. This is possible because the CI seam is before and after the transition state region, where the two diabatic states are degenerate, making more efficient the coupling between them. This explains why below 0.5 eV, the $^3\Sigma^-$ → $^3\Pi$ population is always higher, even when the $^3\Sigma^-$ → $^3\Sigma^-$ probability is very important. For higher energies, above the reaction barrier of the $^3\Sigma^-$ state, this situation becomes more complicated. The $^3\Sigma^-$ → $^3\Sigma^-$ probability becomes very close to that of the $^3\Sigma^-$ → $^3\Pi$, in some cases higher. Accordingly, a similar situation occurs when starting in the $^3\Pi$: the direct $^3\Pi$ → $^3\Pi$ probabilities are higher than the $^3\Pi$ → $^3\Sigma^-$ ones for collision energies below 0.5 eV, because the former has no threshold, while the latter does. Above 0.5 eV, however, the situation reverses as in the previous case.

The importance of the electronic transitions is also illustrated by the resonant structures. In the adiabatic representation, the resonances only appear for the ground $1^3A''$ state, which presents two wells, one in each channel at each side of the reaction barrier, which is the lowest of the two adiabatic states. In the diabatic representation, however, the lower barrier appears for the $^3\Pi$ state, and the two wells are in the $^3\Sigma^-$ state. In this case, the resonances appear in the two diabatic states, suggesting the existence of amplitude in the two wells passing over or across the reaction barrier.

The OH(v = 0) reactant is nearly degenerate with the HF(v' = 3). However, in all cases (except for the $2^3A''$ state), there is a significant vibrational mixing, the most populated v' being 0 at low energies, and v' = 1 for E > 0.4 eV, as can be seen in Figure 3. A nearly vibrational adiabatic mechanism seems to occur. This trend is not so clear below 0.05 eV where the resonant structure dominates. On the contrary, for the excited adiabatic $2^3A''$ state the dominant final vibrational level is v' = 3. The $2^3A''$ adiabatic PES presents a narrow linear barrier, with no wells, so that the exchange reaction dynamics proceeds directly and the final distribution of products is essentially determined by the dynamics in the products channel. In this fast process, there is nearly no rotational excitation, because the collision proceeds at collinear geometries, and the OH colliding with F produces highly vibrating HF products in v' = 3. For the $1^3A''$ or diabatic states the collision takes place at a bent geometry. This makes possible a much higher rotational excitation of the HF products and, at the same time, a much lower vibrational excitation because the collision is less efficient for a translation−vibration energy exchange. In addition, there is a well at each side of the transition state, and therefore the dynamics proceeds mediated by resonances at very low energies.

The rotational distribution for the ground $1^3A''$ adiabatic and the $^3\Sigma^-$ diabatic states is shown in Figure 4, and for the diabatic case the two possible final electronic channels are distinguished. The reaction is very exoergic, by 1.42 eV including zero-point energy, and the HF rotational constant is high, of 2.6 meV. Thus,

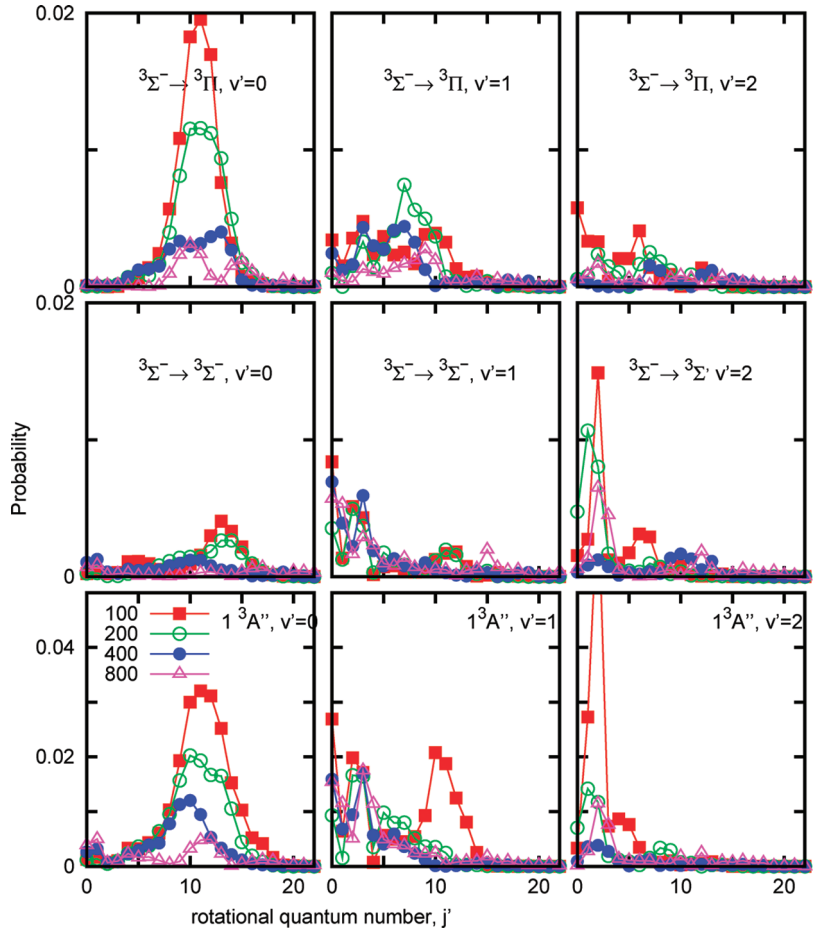

Figure 4. Final rotational reaction probabilities obtained at collisional energies of 100, 200, 400, and 800 meV, for F + OH(v=0,j=0) → O(^{3}P) + HF(v',j') reactive collision at zero total angular momentum, $J = 0$, calculated for the ground adiabatic $1^3A''$ state (bottom panel) and for initially being in the diabatic $^3\Sigma^-$ state but finishing in $^3\Sigma^-$ (middle panel) or $^3\Pi$ state.

the number of open rotational channels does not change significantly for the energies considered, being $j_{max} = 22$, 23, 25, and 28 for $v' = 0$ and $E = 100$, 200, 400, and 800 meV, respectively. The final rotational distribution for $1^3A''$, $v' = 0$ gets colder as energy increases and evolves from a nearly Gaussian distribution at 100 meV peaked at $j' = 11$ to a more structured distribution with a similar mean rotational level. For this reaction in the adiabatic ground state there is no potential barrier but in the diabatic representation, the $^3\Sigma^-$, presents a barrier higher than 0.5 eV, and therefore a double electronic $^3\Sigma^- \rightarrow {}^3\Pi \rightarrow {}^3\Sigma^-$ transition is required to produce HF(v',j') fragments. This complicated path yields a more excited rotational distribution on the $^3\Sigma^-$, $v' = 0$ channel for $E = 100$ and 200 meV, which becomes significantly colder for higher energies. The production of $^3\Pi$, $v' = 0$ only involves a single electronic transition, and for $E = 100$ and 200 meV it is slightly colder than for the $^3\Sigma^-$ case with a nearly Gaussian profile, as in the adiabatic $1^3A''$ case. For $E = 400$ and 800 meV, however, the rotational distribution shows oscillations that do not coincide with those appearing for the adiabatic state.

For $v' = 1$ and 2, the rotational distributions are more complicated, showing several oscillations, suggesting a more complicated energy transfer mechanism. In the $v' = 2$ case the peak appearing for $j' = 2$ for $E = 100$ meV is attributed to a resonance. For the $v' = 1$ state, it seems that $^3\Sigma^-/^3\Pi$ channels imply low/high rotational distributions. For the excited vibrational states, the available kinetic energy is lower, and the system expends more time in the transition state regions, near the CI's, and the electronic mixing then becomes more efficient. Thus the reaction mechanism becomes more complicated.

2. Cross Sections and Rate Constants. The cross sections calculated with the previous adiabatic PES's[33] showed two clear regions: a peak at low energies due to the HLH resonances and a second peak at higher energies attributed to a direct reaction mechanism. In this case, the resonant structures after partial wave sumation transform into a fast increase of the reaction cross section as energy decreases, as shown in Figure 5. Such behavior is typical for reactions without threshold, but in this case at low energies near $E_{col} = 0$ the reaction is not direct but mediated by resonances. The main difference with the previous results[33] is that the second peak associated with the direct mechanism has nearly disappeared in the present case, and only a small shoulder appears at 0.1−0.2 eV. This situation occurs in the adiabatic and diabatic representations and is a consequence of the lowering of the reaction barrier obtained in the PES's shown in Figure 1, due to the correct description of the CI's cusps. The net nonadiabatic effect in this case is the slight increase of the cross section, which for the diabatic representation is nearly always larger than the adiabatic one, especially at low energies, below 0.1 eV, where the resonances seem to dominate.

The present cross sections, both adiabatic and diabatic, are larger than those obtained with the older PES,[32,33] especially around 0.1 eV, the energy region that separates the indirect and direct mechanisms with the old PES. The state specific rate constant calculated with the present diabatic and adiabatic

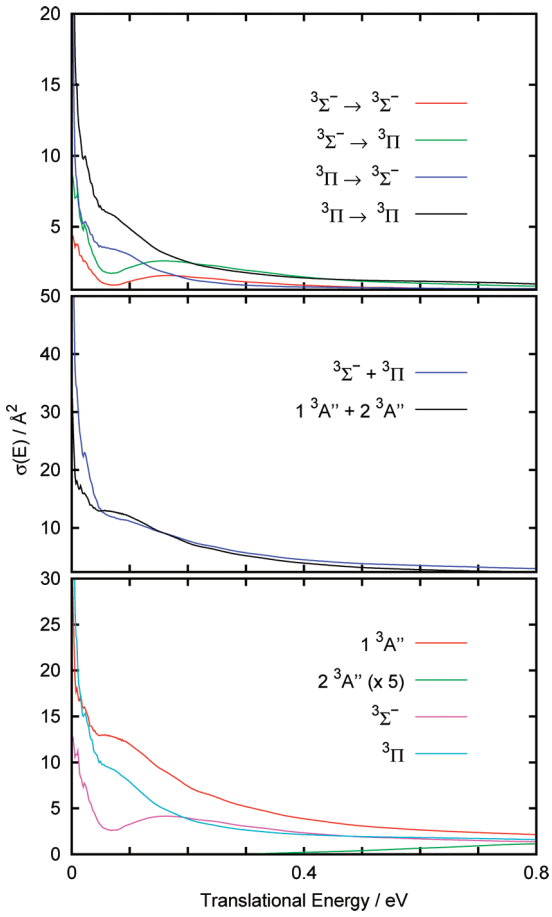

Figure 5. Total reaction cross section obtained for F + OH(v=0,j=0) reactive collision for the adiabatic and the diabatic representations. Bottom panel: total reaction probabilities obtained for the adiabatic $1^3A''$ and $2\ ^3A''$ and diabatic $^3\Sigma^-$ and $^3\Pi$ states. Middle panel: total diabatic versus total adiabatic cross sections. Top panel: diagonal and nondiagonal reaction probabilities obtained in the diabatic representation, for the two initial and final electronic states.

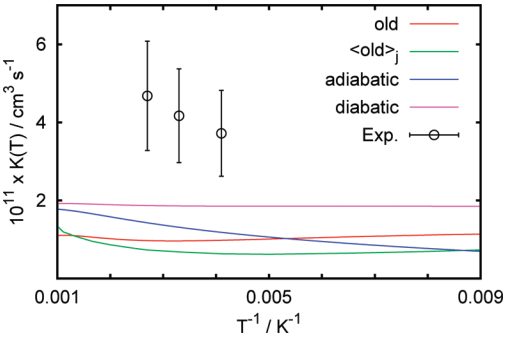

Figure 6. Specific rate constants for the OH(v=0,j=0) + F → O(^{3}P) + HF reaction obtained here in the adiabatic and diabatic representations, summing the contribution of the two electronic states considered here, since the third $1^3A'$ state has a very small contribution. The 3/24 factor due to the electronic degeneracy is considered. The results obtained with the old PES[33] are also included for comparison: for a single rotational state of j = 0 (old) and for a rotational average for a rotational temperature T (<old>$_j$), both multiplied by the electronic factor 3/24. The experimental data are those of ref 37.

representations, in Figure 6, is larger than the one previously calculated,[33] both including the 3/24 factor due to the electronic degeneracy (there are 24 states correlating with the OH + F asymptote, and the triplets correlating with the O(^{3}P) + HF are triply degenerate when spin−orbit effects are neglected). The new adiabatic results are larger, and the inclusion of nonadiabatic effects increases considerably the rate constant specially at low temperatures, where the contribution of low energies is higher. At these energies the reaction occurs through a resonance mediated mechanism. In the coupled diabatic representation, the resonances appear for the two initial electronic states, thus producing a higher rising of the cross section near the threshold. In the adiabatic representation only the ground $1^3A''$ state presents such resonances and hence yields to lower cross sections. In spite of the considerable increase of the rate constants obtained with the coupled diabatic representation, the theoretical results still lie below the experimental results.[37]

Several reasons can be at the origin of this disagreement. First, the PES's used may have some inaccuracies, but the present results use an improvement with respect to the old ones, and it does not seem probable that a significant lowering of the reaction barriers could be achieved by improving the quality of the ab initio calculations. Second, the present results are restricted to the ground rotational levels of the reactants, and hence zero rotational temperature has been considered. However, using WP calculations for OH(v=0,j=1,2,3,4) and QCT calculations from j = 5 to 12, with the old PES, the rotational temperature of reactants was taken into account in ref 33, and the resulting rate constant (<old>$_j$ in Figure 6) is slightly lower, due to a rotational disruption occurring for the lower j 's. Assuming a similar behavior with the present PES's, the rotational averaging does not seem to be the probable reason for the disagreement between theory and experiment.

The disagreement is attributed to the participation of other electronic states that are degenerate in the OH($^2\Pi$) + F(^{2}P) entrance channel (24 degenerate states). First, the remaining $1^3A'$ electronic state is only coupled to the two considered here through electronic Coriolis and Renner−Teller couplings. Its contribution is estimated to be at most on the order of magnitude of the difference between the pure adiabatic and the diabatic results of Figure 6, and hence it is not enough to account for the whole disagreement. Thus, the main reason should be the participation of the other electronic states through spin−orbit couplings.[51−56] These couplings have two major effects on dynamics. First, breaking the degeneracy in the entrance channel,[57] giving rise to a splitting of the 24 states, which modifies considerably the corresponding electronic partition functions. The second effect is the probability of transitions among different electronic states, so that the population of singlet states, when spin−orbit couplings are neglected, can be transferred to triplet states, making the reaction possible. This second effect would require the evaluation of about 24 diabatic PES's and is out of the scope of this work. However, the effect of the splitting of the spin−orbit levels is more accessible and a simple approximation allows us to take it into account in a reasonably way, as was done for other systems like C + OH[56,57] or C + CH.[54]

CAS-SCF calculations have been performed, including spin−orbit couplings using the MOLPRO suite of programs,[58] and the results are shown in Figure 7 for the collinear OHF MEP. The energy curves of the 24 spin−orbit states are shown in the figure, but many of them keep degenerate along the MEP chosen, and others split slightly at a few of the nuclear configurations considered. These calculations do not include dynamic correlation effects showing very important quantitative differences with the MRCI calculations used for the calculation of the diabatic PES's. Clearly, in the OH($^2\Pi$) + F(^{2}P) entrance channel the levels split in four groups, correlating with the F($^2P_{3/2}$) + OH($^2\Pi_{3/2}$), F($^2P_{3/2}$) + OH($^2\Pi_{1/2}$), F($^2P_{1/2}$) + OH($^2\Pi_{3/2}$),

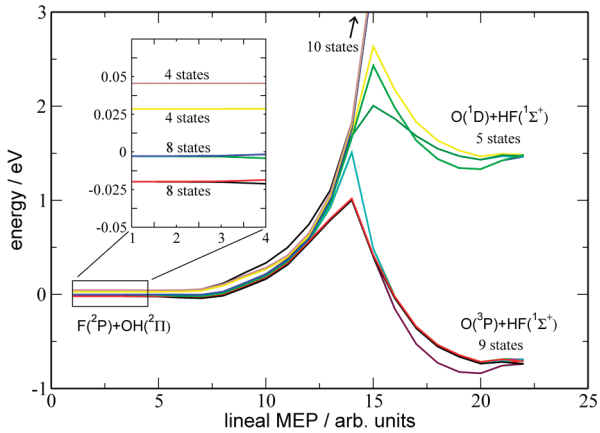

Figure 7. Energies of the 24 states obtained along the 2D meps, at collinear OHF geometry, obtained including the spin−orbit couplings at CAS-SCF level of theory.

and $F(^2P_{1/2}) + OH(^2\Pi_{1/2})$. The 9 triplet states correlating with the $O(^3P) + HF$ product channel essentially correspond to the first 6 states of the ground spin−orbit level and 3 of the first excited one. The latter correspond to the $2^3A'$ adiabatic state and do not contribute significantly to the reaction, as commented above. Therefore, the lowest 6 spin−orbit states can be considered to correlate to the two adiabatic (or diabatic) states considered in this work without spin−orbit couplings.

The asymptotic spin−orbit splitting introduces a major change in the electronic partition function. Considering the experimental splittings (139.2 and 404.1 cm^{-1} for OH and F, respectively), the electronic partition function is given by

$$f_e(T) = g_e e^{-E_e/kT}\left(\frac{1}{4 + 2e^{-404.1/kT}} \times \frac{1}{2 + 2e^{-139.2/kT}}\right) \quad (2)$$

where the energies, E_g, are 0, 139.2, 404.1, and 543.3 cm^{-1} and the degeneracies, g_e, are 8,8,4 and 4, for $e = 1, ..., 4$. k is the Boltzmann constant. These electronic partition factors are shown in the top panel of Figure 8, and if they are divided by g_e they all tend to 1/24 at sufficiently high energies. Each adiabatic ($1^3A''$ and $2^3A''$) or diabatic ($^3\Sigma^-$ and $^3\Pi$) state corresponds to 3 of the 8 degenerate states of the ground manifold, $e = 1$, as discussed above. Thus, to obtain the total rate constant, the contribution of each of those states has to be multiplied by the factor 3/8 f_e, instead of the factor 3/24 used in Figure 6 when no spin−orbit effects were considered. This factor is considerably larger, and the corresponding rate constant, as shown in Figure 8, is also larger than those of Figure 6 without spin−orbit effects. In fact, the diabatic results obtained, including the spin−orbit splitting, are nearly within the experimental error bars and differ considerably from the adiabatic results. This difference demonstrates the necessity of including nonadiabatic effects in this reaction.

The dependence with the temperature is, however, not good since the rate constant decreases with increasing temperature. This fact, however, is partially mitigated when the rotational temperature of the OH reactants is considered, as discussed for Figure 6. Moreover, as temperature increases, other excited states start to be populated and, when couplings among the different spin−orbit states are considered, it is expected that the rate constant increases, in a similar way as happens for the nonadiabatic couplings.

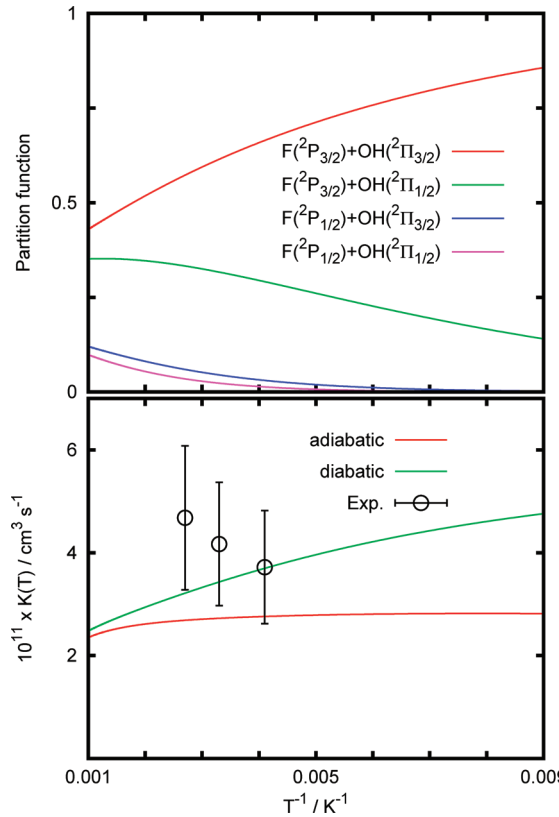

Figure 8. Top panel: electronic partition functions as a function of the inverse of the temperature for the 4 spin−orbit sublevels of the $OH(^2\Pi) + F(^2P)$ asymptote, using the experimental splittings. Bottom panel: adiabatic and diabatic rate constants obtained using the partition function associated to the ground $OH(^2\Pi_{3/2}) + F(^2P_{3/2})$ spin−orbit level.

In the present model potential, the nonadiabatic couplings produce transitions that are remarkable in the electronic resolved integral cross sections shown in the top panel of Figure 5. Thus, when starting in the $^3\Pi$ state, with the lower energy barrier, the dominant final state is also the $^3\Pi$ state, but the cross section corresponding to the $^3\Pi \rightarrow {}^3\Sigma^-$ transition is a significant portion, on the order of one-half to two-thirds of the diagonal one. For the other initial diabatic state, $^3\Sigma^-$, the energy barrier is higher, and the dominant channel corresponds to the nondiagonal $^3\Sigma^- \rightarrow {}^3\Pi$ cross-section, due to the high efficiency of the electronic couplings at the transition state region, where the CI appears leading to nearly degeneracy.

The HF(v') final vibrational state cross sections, in Figure 9, show that in almost all the cases the highest one corresponds to $v' = 1$, decreasing considerably with increasing v', so that $v' = 4$ is nearly negligible. The cross section for producing $v' = 0$ products is the second in importance. In the experiments performed by Sloan et al.[36] the fluorescence of vibrationally excited HF products was detected. The $v = 0$ state could not be detected, but the final probability for $v = 1$ was much higher than for $v = 2$, in agreement with the present results. These results also agree with QCT calculations performed on the old PES for the ground $1^3A''$ adiabatic state, shown if Figure 4 of ref 38.

Only on the excited $2^3A''$ adiabatic state the final vibrational distribution shows a different pattern, for which nearly only $v' = 3$ is formed, which corresponds to the vibrational level nearly degenerate with the OH($v = 0$) vibrational state of the reagents. In this case, approximately all the energy in excess for this exoergic reaction goes to vibration, leading translation and

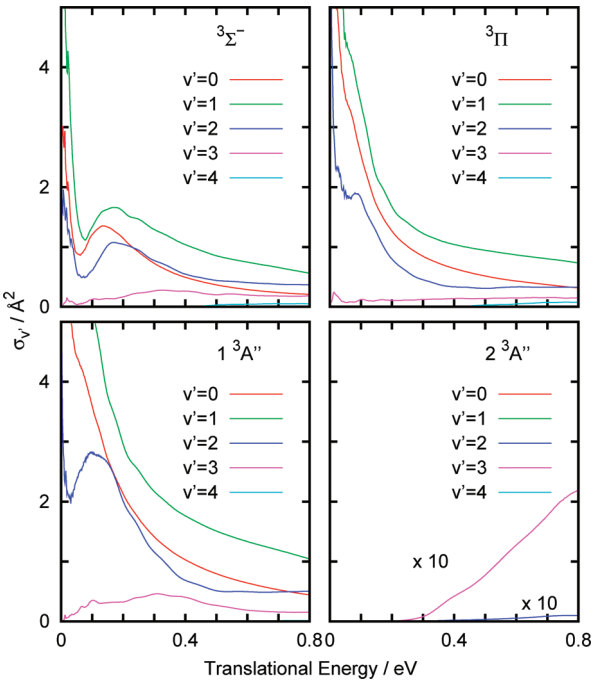

Figure 9. Vibrationally resolved cross sections for the OH(v=0,j=0) + F → O(^{3}P) + HF(v') reaction, obtained for the 1,2^{3}A″ adiabatic states and for the $^3\Sigma^-$ and $^3\Pi$ coupled diabatic states. In the diabatic cases, the cross section for the two possible final electronic states have been added.

rotation nearly equally populated. The reason for this behavior is that the reaction barrier, relatively high at ≈0.5 eV, is at collinear geometries and the PES does not present any well (see Figure 1). Thus, OH directly collides with F, transferring the light H atom when the orientation is favorable. In this process, all energy in excess goes to the light H atom, leading the two heavier atoms at approximately the same speed. This explains why the relative velocity among OH + F and O + HF remains nearly the same, while H is vibrating in the HF products at high speed, leading to highly excited vibrational products.

The cross section for the excited 2^{3}A″ adiabatic state is pretty small and does not contribute significantly to the final vibrational distribution of products in the adiabatic representation, which essentially corresponds to the ground 1^{3}A″ state. In this state, the reaction barrier is much lower, but it presents a bent geometry, which implies a much higher rotation energy transfer in the collision. Because of the large rotational constants, this fact implies that much energy goes to rotation, slowing down the collision process and reducing the vibrational excitation of the HF products. The situation gets more complicated because of the presence of two wells at both sides of the reaction barriers, which gives rise to resonances at which the OHF complex lives for longer periods of time and the energy transfer is more complicated.

In the diabatic representation the situation is similar to that found for the ground 1^{3}A″ adiabatic state, but more complex because of the possibility of electronic transitions between them, due to the electronic couplings.

The rovibrational cross section for the two initial electronic states in the two representations, adiabatic and diabatic, are shown in Figure 10. Again the results obtained for the excited 2^{3}A″ adiabatic state are completely different from all the other cases. For this state only $v' = 3$ is relevant, the rotational distribution is considerably colder than in the other 3 states, for which the vibrational distribution is broader and essentially centered at $v' = 0$, 1, and 2.

For the other three initial electronic states, the rotational distributions are rather similar among them, showing a progressive lowering of the rotational distribution as v' increases. If the cross sections obtained for the two initial diabatic states are added, the total distribution becomes very similar to that of the ground 1^{3}A″ adiabatic state. For $v' = 0$ the distribution is nearly Gaussian and centered at about $j' = 12$, and with increasing energy the distribution becomes broader but not significantly more excited. For $v' = 1$, there is a bimodal rotational distribution, with a peak centered at $j' = 2$ and another one at $j' = 8-12$. As energy increases, the peaks become broader, and the relative importance shifts from the more excited toward the lower rotational peak. A similar behavior also appears for $v' = 2$ and in a lower extent to $v' = 0$. These results are surprising since the rotational excitation seems to decrease as available energy increases.

Let us start by using the adiabatic representation to explain these findings. For the ground 1^{3}A″ state, the transition state is bent. Therefore, for the low translational energy the reaction occurs at bent geometries at which the diatomic rotational excitation is enhanced. However, as the energy increases the collinear geometry becomes accessible, being in the center of the angular cone of acceptance, shown in the bottom right panel of Figure 1. Thus, when the collision occurs at these quasilinear geometries, the rotational excitation becomes lower, approaching what happens in the excited 2^{3}A″ adiabatic state, which presents a collinear transition state.

The rotational distribution obtained here for the lower rotational states of the OH fragments is rather narrow as compared with the experimental ones,[36] specially for $v' = 0$. However, when the initial OH rotational temperature is included, such distributions become broader and closer to the experimental ones; see Figure 5 of ref 38.

IV. Conclusions

In this work we present a detailed wave packet study of the nonadiabatic reaction dynamics of the OH($^2\Pi$) + F(^{2}P) → O(^{3}P) + HF($^1\Sigma^+$) collisions, using recently proposed coupled diabatic PES's,[25] comparing in detail with the results obtained with the associated adiabatic PES's. These diabatic PES's are regular at the conical intersections that appear along the MEP near the reaction barriers. The dynamics involves several transitions among the two diabatic states. Within the coupled diabatic representation the reaction cross sections are considerably higher than those obtained with the adiabatic representation. This situation is especially important at low energies where the resonance-mediated mechanism dominate. In the diabatic representation the two states are coupled and such a mechanism takes place for the two initial $^3\Sigma^-$ and $^3\Pi$ states. In the adiabatic representation, however, only the ground 1^{3}A″ state presents resonant structures. Therefore, the overall increase of the reaction cross section is attributed to the nonadiabatic effects near the conical intersection seams.

In addition, the diabatic and adiabatic cross sections obtained in this work are higher than those previously reported obtained using different PES's.[33]

Thus the reaction rate constants obtained here are also higher than those previously reported. In addition, the diabatic rate constant obtained here is particularly larger than the adiabatic one, especially at low temperatures where the weight of the resonances is more important. However, the values obtained are still lower than the experimental values so far reported[37] if spin−orbit effects are not taken into account.

The disagreement is attributed to the spin−orbit effects that couple the triplet state considered in this work with the singlet

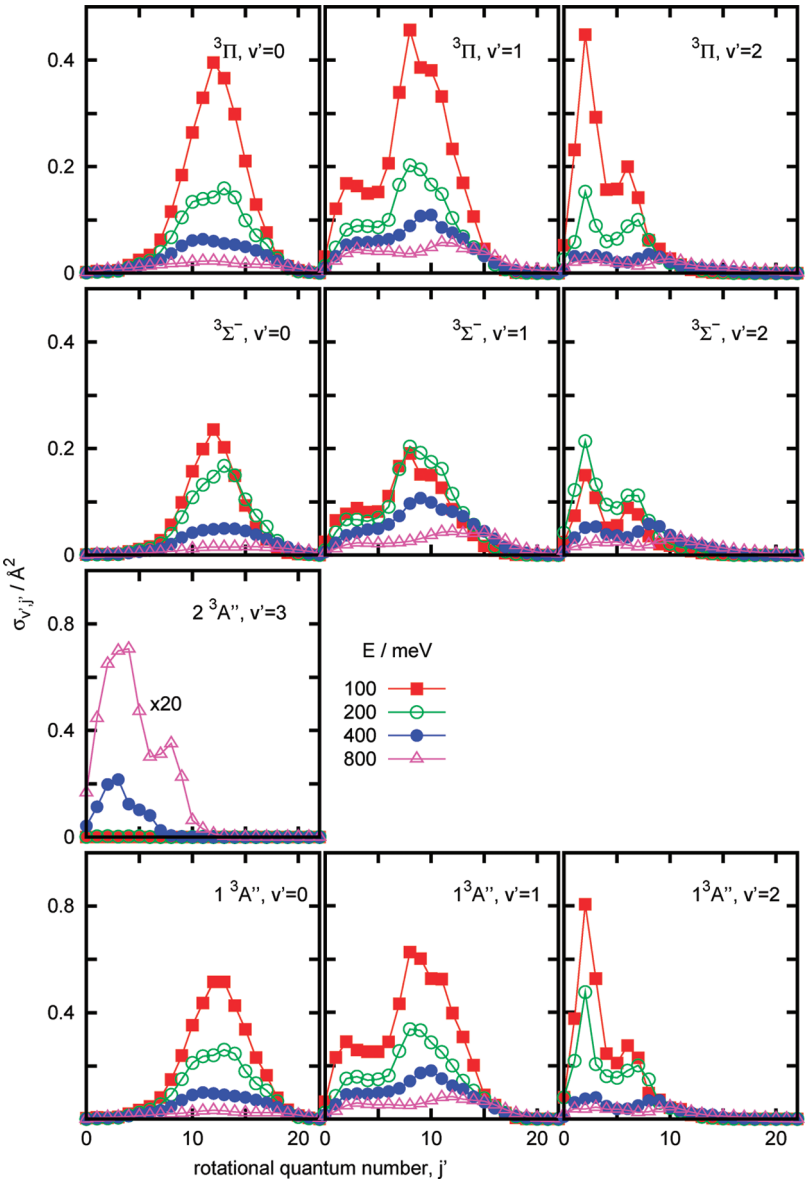

Figure 10. Rotationally resolved cross sections for the OH(v=0,j=0) + F → O(^{3}P) + HF(v',j') reaction, obtained for the 1,2^{3}A″ adiabatic states and for the $^3\Sigma^-$ and $^3\Pi$ coupled diabatic states. In the diabatic cases, the cross section for the two possible final electronic states have been added.

state correlating to the O(^{1}D) + HF fragments. When the spin−orbit splitting is taken into account, the electronic partition function for the triplet states increases, considerably leading to results in near agreement with the experimental ones available.

Moreover, the singlet states are degenerate with the triplet states in the entrance channel, making the spin−orbit couplings very effective, and are expected to induce electronic transitions among them which would increase the reactivity. Nevertheless, more experimental results on this system would be desirable for a better comparison.

In this regard, the new experiments with hyperthermal O(^{3}P) atoms[59−62] would allow us to study the reverse reaction, even when such a reaction is endothermal by 1.5 eV. In such a process the spin−orbit affects only the OH($^2\Pi$) + F(^{2}P) exit channel where all the states get together, without varying the total reaction cross sections. In such a situation the reaction dynamics is expected to be well represented by the diabatic PES's used in this work. A theoretical simulation of such a process is nowadays undertaken.

Acknowledgment. This work has been supported by Ministerio de Ciencia e Innovación under Project Nos. CTQ2007-62898 and CTQ2007-63332. The calculations have been performed at CESGA supercomputing center.

References and Notes

(1) Zhang, J.; Head-Gordon, M. Editorial, special issue. *Phys. Chem. Chem. Phys.* **2009**, *11*, 4699.
(2) Schinke, R.; McBane, G. C.; Shen, L.; Singh, P. C.; Suits, A. G. *J. Chem. Phys.* **2009**, *131*, 011101.
(3) Grebenshchikov, S. Y.; Qu, Z.-W.; Zhu, H.; Schinke, R. *Phys. Chem. Chem. Phys.* **2007**, *9*, 2044.
(4) Wayne, R. P. *Chemistry of Atmospheres*, 2nd ed.; Clarendon Press: Oxford, U.K., 2000.
(5) Ivanov, M.; Zhu, H.; Schinke, R. *J. Chem. Phys.* **2007**, *126*, 054304.
(6) Dobbyn, A. J.; Knowles, P. J. *Mol. Phys.* **1997**, *91*, 1107.
(7) Drukker, K.; Schatz, G. C. *J. Chem. Phys.* **1999**, *111*, 2451.
(8) Gray, S. K.; Balint-Kurti, G.; Schatz, G. C.; Lin, J. J.; , X.; Liu, S. H.; Yang, X. *J. Chem. Phys.* **2000**, *113*, 7330.
(9) Aoiz, F. J.; Bañares, L.; Castillo, J. F.; Brouard, M.; Denzer, W.; Vallance, C.; Honvault, P.; Launay, J.-M.; Dobbyn, A. J.; Knowles, P. J. *Phys. Rev. Lett.* **2001**, *86*, 1729.
(10) Balakrishnan, N. *J. Chem. Phys.* **2004**, *121*, 6346.

(11) Chu, T.-S.; Zhang, X.; Han, K.-L. *J. Chem. Phys.* **2005**, *122*, 214301.
(12) Lin, S. Y.; Guo, H. *J. Phys. Chem. A* **2009**, *113*, 4285.
(13) Braunstein, M.; Adler-Golden, S.; Maiti, B.; Schatz, G. C. *J. Chem. Phys.* **2004**, *120*, 4316.
(14) Ravishankara, A. R.; Smith, G.; Watson, R.; Davis, D. *J. Phys. Chem.* **1977**, *81*, 2220.
(15) Macdonald, R.; Moore, C. B. *J. Chem. Phys.* **1978**, *68*, 513.
(16) Rakestraw, D.; MacKendrick, K.; Zare, R. N. J. Chem. Phys. 1987, *87*, year.
(17) Mahmud, K.; Kim, J.-S.; Fontijn, A. *J. Phys. Chem.* **1990**, *94*, 2994.
(18) Zhang, R.; van der Zande, W.; Bronikowski, M. J.; Zare, R. N. *J. Chem. Phys.* **1991**, *94*, 2704.
(19) Koizumi, H.; Schatz, G.; Gordon, M. S. *J. Chem. Phys.* **1991**, *95*, 6421.
(20) Ramachandran, B.; Schrader, E. A., III; Senekowitsch, J.; Wyatt, R. E. *J. Chem. Phys.* **1999**, *111*, 3862.
(21) Aoiz, F.; Bañares, L.; Castillo, J.; Menéndez, M.; Verdasco, J. *Phys. Chem. Chem. Phys.* **1999**, *1*, 1149.
(22) Nobusada, K.; Nakamura, H.; Lin, Y.; Ramachandran, B. *J. Chem. Phys.* **2000**, *113*, 1018.
(23) Xie, T.; Bowman, J. M.; Peterson, K. A.; Ramachandran, B. *J. Chem. Phys.* **2003**, *119*, 9601.
(24) Ramachandran, B.; Peterson, K. A. *J. Chem. Phys.* **2003**, *119*, 9590.
(25) Gómez-Carrasco, S.; Aguado, A.; Paniagua, M.; Roncero, O. *J. Chem. Phys.* **2006**, *125*, 164321.
(26) Bradforth, S.; Arnold, D.; Metz, R. B.; Weaver, A.; Neumark, D. *J. Phys. Chem.* **1991**, *95*, 8066.
(27) Bradforth, S. E. *Ph.D. Thesis*, University California, Berkeley, 1992.
(28) Neumark, D. M. *Phys. Chem. Chem. Phys.* **2005**, *7*, 433.
(29) Deyerl, H.-J.; Continetti, R. E. *Phys. Chem. Chem. Phys.* **2005**, *7*, 855.
(30) Continetti, R. E. Private communication, 2005.
(31) Dixon, R. N.; Tachikawa, H. *Mol. Phys.* **1999**, *97*, 195.
(32) Gómez-Carrasco, S.; González-Sánchez, L.; Aguado, A.; Roncero, O.; Alvariño, J. M.; Hernández, M. L.; Paniagua, M. *J. Chem. Phys.* **2004**, *121*, 4605.
(33) Gómez-Carrasco, S.; Roncero, O.; González-Sánchez, L.; Hernández, M. L.; Alvariño, J. M.; Paniagua, M.; Aguado, A. *J. Chem. Phys.* **2005**, *123*, 114310.
(34) González-Sánchez, L.; Gómez-Carrasco, S.; Aguado, A.; Paniagua, M.; Hernández, M. L.; Alvariño, J. M.; Roncero, O. *J. Chem. Phys.* **2004**, *121*, 9865.
(35) Gomez-Carrasco, S.; Hernández, M.; Alvariño, J. *Chem. Phys. Lett.* **2007**, *435*, 188.
(36) Sloan, J. J.; Watson, D. G.; Williamson, J. M.; Wright, S. *J. Chem. Phys.* **1981**, *75*, 1190.
(37) Walter, C. D.; Wagner, H. G. *Ber. Bunsen-Ges. Phys. Chem.* **1983**, *87*, 403.
(38) Gómez-Carrasco, S.; González-Sánchez, L.; Aguado, A.; Paniagua, M.; Roncero, O.; Hernández, M. L.; Alvariño, J. M. *Chem. Phys. Lett.* **2004**, *383*, 25.
(39) Gogtas, F. *J. Comput. Chem.* **2008**, *29*, 1889.
(40) Chu, T. S.; Zhang, H.; Yuan, S.; Fu, A.; Si, H.; Tian, F.; Duan, Y. *J. Phys. Chem. A* **2009**, *113*, 3470.
(41) Zhao, J.; Xu, Y.; Yue, D.; Meng, Q. *Chem. Phys. Lett.* **2009**, *471*, 160.
(42) Meng, Q.; Zhao, J.; Xu, Y.; Yue, D. *Chem. Phys.* **2009**, *362*, 65.
(43) Aguado, A.; Paniagua, M.; Lara, M.; Roncero, O. *J. Chem. Phys.* **1997**, *107*, 10085.
(44) Lara, M.; Aguado, A.; Roncero, O.; Paniagua, M. *J. Chem. Phys.* **1998**, *109*, 9391.
(45) González-Lezana, T.; Aguado, A.; Paniagua, M.; Roncero, O. *J. Chem. Phys.* **2005**, *123*, 194309.
(46) Gómez-Carrasco, S.; Roncero, O. *J. Chem. Phys.* **2006**, *125*, 054102.
(47) Zanchet, A.; Roncero, O.; González-Lezana, T.; Rodrguez-López, A.; Aguado, A.; Sanz-Sanz, C.; Gómez-Carrasco, S. *J. Phys. Chem. A* **2009**, *113*, 14488.
(48) Bowman, J. M. *Adv. Chem. Phys.* **1985**, *61*, 115.
(49) http://www.iff.csic.es/fama/personas/octavio/metodos programas/PES/PES.html, 2010.
(50) Rebentrost, F.; Lester, W. A., Jr. *J. Chem. Phys.* **1976**, *64*, 3879.
(51) Schatz, G. C. *J. Phys. Chem.* **1995**, *99*, 7522.
(52) Alexander, M. H.; Werner, H.-J.; Manolopoulos, D. E. *J. Chem. Phys.* **1998**, *109*, 5710.
(53) Whiteley, T. W. J.; Dobbyn, A. J.; Connor, J.; Schatz, G. C. *Phys. Chem. Chem. Phys.* **2000**, *2*, 549.
(54) Boggio-Pasqua, M.; Voronon, A. I.; Halvick, P.; Rayez, J.-C. *Phys. Chem. Chem. Phys.* **2000**, *2*, 1693.
(55) Zanchet, A.; Halvick, P.; Rayez, J.-C.; Bussery-Honvault, B.; Honvault, P. *J. Chem. Phys.* **2007**, *126*, 184308.
(56) Zanchet, A.; Halvick, P.; Bussery-Honvault, B.; Honvault, P. *J. Chem. Phys.* **2008**, *128*, 204301.
(57) Bussery-Honvault, B.; Dayou, F.; Zanchet, A. *J. Chem. Phys.* **2008**, *129*, 234302.
(58) MOLPRO is a package of ab initio programs designed by H.-J. Werner and P. J. Knowles and with contributions from and J. Almlöf and R. D. Amos and A. Berning and M. J. O. Deegan and F. Eckert and S. T. Elbert and C. Hampel and R. Lindh and W. Meyer and A. Nicklass and K. Peterson and R. Pitzer and A. J. Stone and P. R. Taylor and M. E. Mura and P. Pulay and M. Schütz and H. Stoll and T. Thorsteinsson and D. L. Cooper, version 2006.
(59) Garton, D. J.; Minton, T. K.; Maiti, B.; Troya, D.; Schatz, G. C. *J. Chem. Phys.* **2003**, *118*, 1585.
(60) Brunsvold, A. L.; , J.; Zhang, H. P. U.; Minton, T. K.; Camden, J. P.; Paci, J. T.; Schatz, G. C. *J. Phys. Chem. A* **2007**, *111*, 10907.
(61) Brunsvold, A. L.; Upadhyaya, H. P.; Zhang, J.; Cooper, R.; Minton, T. K.; Braunstein, M.; Duff, J. W. *J. Phys. Chem. A* **2008**, *112*, 2192.
(62) Garton, D. J.; Minton, T. K.; Hu, W.; Schatz, G. C. *J. Phys. Chem. A* **2009**, *113*, 4722.

JP101914A